Articles

Circular RNA circR-4600 inhibits hepatocellular carcinoma progression by suppressing autophagy through DVL3 and DAB2 interaction

DOI:https://dx.doi.org10.71373/XEDR3565
Submitted 19November2025
Accepted 26 December 2025
Published 31 December 2025

Gang Wang[1#], Shaoliang Zhu[2#], Zhizhong Chen[3#], Yulin Yuan[4#], Qiuxia Wei[1], Hongwei Wang[5], Tao Yang[1], Ling Cai[1], Xiaosu Zou[1], Wenqian Nong[1], Qicong Chen[1], Lequn Li[6], Xiaofeng Dong[2], Feixiang Wu[6§], Honglin Luo[1§]

Circular RNA (circRNA) plays a crucial role in regulating autophagy in hepatocellular carcinoma (HCC); however, the specific mechanisms underlying this regulation remain poorly understood. This study investigates the role and mechanisms of circR-4600 in HCC, aiming to identify novel therapeutic targets to enhance patient prognosis. Differential expression of circRNA in HCC and adjacent non-tumor tissues from six patients was assessed using circRNA microarray analysis. RNA pulldown combined with ESI-FT-ICR-MS identified DVL3 as the RNA-binding protein that interacts with circR-4600. Functional assays, including overexpression and knockdown experiments in HCC cell lines, as well as *in vivo* studies, were conducted to evaluate the effects. The results demonstrated significantly lower circR-4600 expression in HCC tissues, which negatively correlated with poor prognosis. Overexpression of circR-4600 inhibited HCC cell proliferation, migration, and invasion *in vitro*, and reduced lung metastasis *in vivo*. Mechanistically, circR-4600 interacted with DVL3 and suppressed ATG5-mediated autophagy. This effect attenuated the inhibitory activity of DVL3 on DAB2, resulting in reduced LC3B expression, inhibition of epithelial-mesenchymal transition, and increased P62 accumulation.In conclusion, circR-4600 modulates autophagy through DVL3 and DAB2, thereby inhibiting HCC progression and providing insights into its potential as a therapeutic target.

Introduction

Hepatocellular carcinoma (HCC) is one of the most common malignant tumors worldwide, with high incidence and mortality rates[1]. Despite some progress in early diagnosis and treatment of HCC, the complexity of its biological characteristics poses significant challenges to the treatment[2,3]. Autophagy is a cellular process that eliminates and recycles damaged organelles and proteins, enabling tumor cells to adapt to nutrient scarcity while helping to maintain cellular homeostasis and resist stress[4]. Recent evidence indicates that autophagy influences HCC progression by degrading essential molecules involved in the epithelial-mesenchymal transition (EMT) process, thereby modulating the expression and activity of EMT-related transcription factors[5]. EMT is believed to assist tumor cells in escaping the primary tumor and entering the bloodstream to form circulating tumor cells (CTCs), ultimately allowing them to reach distant sites and establish metastases[6].

1. Institute of Oncology, Guangxi Academy of Medical Sciences, Nanning, Guangxi, 530021, China. 2. Department of Hepatobiliary, Pancreas and Spleen Surgery, People's Hospital of Guangxi Zhuang Autonomous Region, Nanning, Guangxi, 530021, China. 3. Joint Inspection Center of Precision Medicine, People's Hospital of Guangxi Zhuang Autonomous Region & Guangxi Academy of Medical Sciences, Nanning, Guangxi, 530021, China. 4. Department of Laboratory Medicine, The People's Hospital of Guangxi Zhuang Autonomous Region, The Guangxi Key Laboratory of intelligent precision medicine, Nanning, Guangxi Zhuang Autonomous Region, 530021, China. 5. State Key Laboratory of Analytical Chemistry for Life Science, Medical School of Nanjing University, Nanjing, China. 6. Department of Hepatobiliary Surgery, Guangxi Medical University Cancer Hospital, Nanning, Guangxi, 530021, China.

Running title: circR-4600 suppresses HCC progression by autophagy.

 # Gang Wang, Shaoliang Zhu, Zhizhong Chen, and Yulin Yuan contributed equally to this paper.

§ Corresponding authors:
Prof. Honglin Luo (Email: lhl200296@126.com).
Prof. Feixiang Wu (Email: wufx2013@163.com).

In recent years, circular RNAs (circRNAs) have emerged as key regulators of diverse biological processes, including gene expression, protein translation, and tumorigenesis[7-9]. CircRNA participates in these processes through various mechanisms, including interacting with RNA-binding proteins (RBPs) at distinct binding sites, influencing post-transcriptional modifications and protein expression, thereby affecting cancer malignancy[10,11]. Given the significant role of circRNA in tumors, it may serve as a novel target for cancer diagnosis and treatment. Additionally, the potential application of circRNA as a biomarker in tumor diagnosis shows considerable promise. Accumulating evidence has demonstrated that circRNAs are involved in HCC progression by regulating autophagy through acting as a sponge for miRNA, regulating gene expression by affecting the function of miRNA[12-14]. However, the regulation of autophagy by circRNA through binding to RBPs in HCC has not been reported.

DVL3, a core effector protein in the WNT signaling pathway, is highly expressed in HCC[15]. It exerts control over tumor invasion and metastasis through multiple mechanisms, including activation of the PI3K/Akt signaling pathway, inhibition of the Hippo signaling pathway, and induction of EMT[16,17]. There is a complex interaction network between DVL3 and circRNA in tumors. circRNA regulates the expression and activity of DVL3 through a variety of pathways[18]. However, the regulatory mechanisms of DVL3 mediating by circRNA to affect HCC progression remain unknown.

During the investigation into the malignant biological behaviors of HCC cells, we identified a circRNA(circR-4600, hsa_circ_0005927) based on the circRNA microarray analysis within the tumor tissues of HCC patients. It was observed that the expression of circR-4600 was down-regulated in HCC tissues, and this was associated with a poor prognosis. Overexpressing circR-4600 markedly suppressed proliferation, invasion, and metastasis of HCC *in vitro* and *in vivo*. A comprehensive exploration of functional and molecular mechanisms further elucidated the interaction between circR-4600 and DVL3. In detail, overexpression of circR-4600 not only inhibited DVL3 expression but also suppressed the expression of LC3B and promoted P62 accumulation in HCC. Mechanistically, circR-

4600 inhibited the expression of DVL3 after binding to DVL3, thereby weakening the inhibitory effect of DVL3 on DAB2, weakening ATG5-mediated autophagy, inhibiting EMT, and further inhibiting HCC progression. This pivotal discovery underscores the intricate role of circRNA in HCC and its regulatory function in key pathways. The study offers a fresh perspective for a more profound understanding of HCC pathogenesis and lays a theoretical foundation for the development of treatment strategies targeting circR-4600.

Materials and Methods

Circular RNA microarray screening for target circular RNAs

Arraystar Human circRNA Array analysis was conducted on 6 cases of HCC tissues and corresponding adjacent non-tumor tissues. Total RNA from each sample was quantified using NanoDrop ND-1000. Sample preparation and microarray hybridization were performed following Arraystar's standard protocol. Briefly, total RNA was digested with Rnase R (Epicentre, Inc.) to remove linear RNA and enrich circular RNA. Subsequently, the enriched circular RNA was amplified and transcribed into fluorescent cRNA using the random priming method (Arraystar Super RNA Labeling Kit; Arraystar). The labeled cRNAs were purified using the RNeasy Mini Kit (Qiagen) to measure the concentration and specific activity of labeled cRNAs using NanoDrop ND-1000. Each labeled cRNA (1μg) was fragmented by adding 5 μl 10 × Blocking Agent and 1 μl of 25 × Fragmentation Buffer, heating the mixture at 60℃ for 30 minutes, and then adding 25 μl 2 × Hybridization Buffer to dilute the labeled cRNA. Fifty microliters of hybridization solution were dispersed onto the circRNA expression microarray slide and assembled. The slide was incubated at 65℃ for 17 hours in an Agilent Hybridization Oven. After hybridization, the array was washed, fixed, and scanned using the Agilent Scanner G2505C. Subsequently, scanned images were imported into Agilent Feature Extraction software for raw data extraction. Quantile normalization and subsequent data processing of the raw data were performed using the R software package. After quantile normalization of the raw data, low-intensity filtering was performed, and circRNAs with "P" or "M" ("All Targets Value") flags present in at least 6 samples were retained for further analysis. When comparing the differences in profiles between HCC and control groups, the "fold change" (i.e., the ratio of group averages) for each circRNA was calculated. The statistical significance of differences was estimated using *t*-tests. CircRNAs with fold changes greater than or equal to 1.5 and *P*-values less than 0.05 were selected as significantly differentially expressed.

RT-qPCR detection

In this study, tissue samples weighing between 50 and 100 mg were homogenized using the TRIZOL reagent (Invitrogen). Chloroform was then added to effectively separate RNA from other components, ensuring complete transfer of RNA to the aqueous phase. The RNA was precipitated using isopropanol and the precipitate was cleaned with 75% ethanol, prepared with DEPC-treated water. The RNA precipitate was dissolved in RNase-free water and stored at -80°C for future use. The concentration and purity of the RNA were measured using the NanoDrop® ND-1000 instrument, and the quality of the RNA was evaluated through denaturing agarose gel electrophoresis. cDNA synthesis was carried out using SuperScript™ III reverse transcriptase (Invitrogen), an RNase inhibitor (Epicentre), 5 × RT buffer (Invitrogen), and N6 random primers. For the reverse transcription of mRNA, a reverse transcription kit (TAKARA, Japan) was utilized. The RT-qPCR analysis was conducted using a 2 × PCR master mix (Arraystar), and the PCR reaction was completed using the ViiA 7 Real-time PCR System (Applied Biosystems). The sequences of the primers are provided in Supplementary Table 1. The relative levels of RNA were calculated using the comparative CT ($2^{-\Delta\Delta Ct}$) method.

Fluorescence in situ hybridization (FISH) localization of circR-4600 in HCC cells

The spatial distribution of circR-4600 within SMMC7721 cells was delineated utilizing FISH technology. Before the commencement of the experiment, preparations were made for reagents, including the circR-4600 probe, Anti-Dig-red, hybridization fluid, DAPI, Rubber Cement, and a 3% BSA sealing solution. Concurrently, solutions such as 0.1M HCl, 0.5% TritonX-100, and a fixative were prepared. The sequence of the probe was established as 5'-3' GGCCTTCAATTTCCCACTCTTCTTTAG AGAGAGAAGTTCTACAAT. The cells were initially fixed using a fixative, formulated by combining methanol and glacial acetic acid in a 3 : 1 ratio, followed by a wash with a 2 × SSC solution containing 0.1% NP-40. A 0.5% TritonX-100 solution was employed for cell permeabilization, facilitating probe penetration. Subsequently, the cells were once again fixed with a 4% paraformaldehyde solution to preserve cellular structural integrity. The probe was denatured at 88°C for 5 minutes, swiftly cooled to 4°C to form a single-strand structure, and then diluted in a 1 : 100 ratio in a preheated (55°C) hybridization solution. The hybridization reaction was condu- cted overnight in a humid box at 37°C, ensuring optimal probe- target RNA binding. Post-hybridization, the cells underwent multiple washes with a 1 × PBS solution containing 0.1% DEPC, effectively removing non-specifically bound probes. The cells were then treated with a 3% BSA sealing solution for 30 minutes to obstruct non-specific binding sites. Subsequently, Anti-Dig-red was employed for probe detection. This detection reagent was diluted in a 1:100 ratio with 1% BSA, added to the cells, and incubated in the dark at 37°C for 1 hour. The cells were then stained with DAPI, covered with a cover slip, and placed in the dark for 20 minutes to minimize photobleaching. Ultimately, image results were acquired via a CSM 700 laser confocal microscope.

Analysis of the correlation between circR-4600 and clinical prognosis

An analysis was conducted to examine the correlation between circR-4600 and clinical prognosis. The study incorporated 222 patients, postoperatively diagnosed with HBV-associated HCC. Because this was a retrospective observational study, the sample size was determined by the number of consecutive eligible patients available during the study period. Histopathological examinations were performed on all patients, ensuring adherence to the diagnostic standards set by the National Comprehensive Cancer Network (NCCN) for tumor clinical practice. To acquire comprehensive patient data, telephonic or in-patient follow-ups were conducted until the patient's demise or the final follow-up. The median follow-up duration extended to 17 mont-

hs, with a range of 3 to 32 months, thereby ensuring data accuracy. During the screening phase, meticulous attention was given to confirm the absence of prior cancer diagnoses among patients, thereby eliminating potential confounding factors. Detailed patient records were maintained, encompassing age, gender, pathological grading, tumor biological behavior, serum alpha-fetoprotein (AFP) levels, cirrhosis status, and whether radical resection was performed, among other clinicopathological characteristics. To gain a comprehensive understanding of the patient's tumor status, the Barcelona Clinical Liver Cancer (BCLC) staging system was employed for tumor classification. This system considers various factors, including the patient's liver function, tumor size and number, and the presence of vascular invasion. The patient enrollment flowchart is shown in Supplementary Figure 1.

Plasmid construction and lentiviral packaging

The construction of plasmids and the packaging of lentiviruses were carried out as follows. The flanking sequences of the mature circR-4600 sequence were compared in the circBase database. An additional 365 bp was appended to the 5' end, and 416 bp to the 3' end, resulting in a total sequence of 1160 bp for the vector, inclusive of the 379 bp mature circR-4600 sequence. The full-length 1160 bp sequence was synthesized using the whole gene synthesis method and subsequently incorporated into the pCDH-CMV-MCS-EF1-GFP+Puro (CD513B-1) vector via EcoRI and BamHI linkages. Upon completion of the linkage, the recombinant plasmid was screened and verified. Total RNA was extracted from the cell samples and subjected to RT-qPCR detection. This process involved the use of an internal reference, circular RNA-specific primers (Divergent primers), and corresponding linear sequence primers (Convergent primers). Sequencing primers were also designed, and post-PCR, the bands were recovered and sequenced to verify the junction of the circularization site. The sequences of these primers are provided in Supplementary Table 2. Subsequently, lentivirus packaging was conducted using 293T cells. Small or short interfering RNA (siRNA) inhibition technology was employed to construct DVL3 and ATG5 inhibitory lentiviruses. siRNA sequences, specifically targeting DVL3 and ATG5, were designed. These sequences were capable of precisely binding to the target mRNA, thereby inhibiting its translation process. The corresponding siRNAs for DVL3 and ATG5 are as follows: DVL3-homo:CCAGGAGAACCUGGACAAUTT; ATG5-homo: CCA UCAAUCGGAAACUCAUTT. These siRNA sequences were then individually incorporated into the lentivirus genome, resulting in the construction of DVL3 and ATG5 inhibitory lentiviruses. The effectiveness and specificity of these lentiviruses were confirmed by infecting various HCC cells and assessing the expression levels of DVL3 and ATG5.

Assessment of cell proliferation using BrdU and CCK-8 assays

Two commonly used methods for assessing cell proliferation are the BrdU (5-bromo-2'-deoxyuridine) assay and the CCK-8 (Cell Counting Kit-8) assay. In this study, we employed these techniques to investigate cell growth in HCC cells.

BrdU Assay: HCC cells were suspended in DMEM medium supplemented with 10% fetal bovine serum (FBS, Gibco, USA) and a 1% mixture of penicillin-streptomycin (Solarbio, China). After re-suspension, the cells were cultured at 37℃ with 5% CO2. Transient transfection was performed in 6-well plates. The day before transfection, 5 × 10^5 cells were seeded in culture plates and incubated with 2 ml complete growth medium to achieve 70-90% confluence. Plasmid DNA (3 μg) was gently mixed with 100 μl serum-free medium. Lipofectamine 3000 reagent was diluted with 100 μl serum-free medium containing 4 μl Lipofectamine 3000 and incubated at room temperature for 5 minutes. The diluted plasmid and Lipofectamine 3000 were combined and incubated for 20 minutes to form the plasmid-Lipofectamine 3000 complex. The complex was added to cell wells containing 800 μl serum-free medium, followed by gentle shaking. After 5-6 hours of incubation at 37℃ with 5% CO2, the transfection medium was aspirated, and complete growth medium was replaced.

CCK-8 Assay: The CCK-8 assay (Beyotime, China) was used to assess cell viability. Briefly, 10000 cells were seeded in 100 μl DMEM medium per well. Next, 10 μl of CCK-8 solution was added to each well, followed by a 2-hour incubation. Absorbance was measured at 450 nm using a microplate reader.

Cell migration, invasion, and clonogenic assays

Cell migration experiments (scratch assays) primarily involve creating scratches on a cell culture plate and observing how cells fill these scratches to assess their migration ability. First, evenly mark horizontal lines on the back of a 6-well plate using a marker. Then, add fibronectin to each well. After seeding the cells, treat them with cytosine arabinoside for one hour to inhibit cell division. Next, create scratches on the cell culture plate and wash with PBS to remove dislodged cells. Finally, use ImageJ software to measure scratch width at eight arbitrary locations for each cell group at the same time point and calculate cell migration distance.

The detection of cell invasion ability typically employs the Transwell assay. Initially, dissolve matrigel matrix gel at 4℃ and dilute it with pre-chilled serum-free medium. Add this mixture to pre-chilled Transwell chambers and incubate at 37℃ to allow matrigel to solidify. Subsequently, introduce cells into the upper chamber of the Transwell. After 24 and 48 hours of incubation at 37℃ with 5% CO2, remove the chambers, wipe off cells from the upper chamber using a cotton swab, fix with 4% paraformaldehyde, wash with PBS, and stain with crystal violet for 10 minutes. Finally, assess whether cells have penetrated the pores by capturing images.

The plate clonogenic assay evaluates cell clonogenic formation ability by seeding a small number of cells in a culture plate and observing their growth and division. Digest cells in logarithmic growth phase with trypsin, resuspend them in complete culture medium, and count. Then, seed 1000 cells in a 6-well culture plate. Continue cultivation for 14 days or until the majority of single-cell clones contain more than 50 cells. During this period, change the medium every 3 days and monitor cell status. After completing clonogenic growth, photograph the cells under a microscope, wash with PBS, fix with 4% paraformaldehyde for 30 minutes, stain with crystal violet for 20 minutes, rinse with PBS, air-dry, and capture images using a camera.

In vivo assessment of tumor formation following lentiviral particle infection with circR-4600 in

mice

In this study, we investigated the impact of circR-4600 on tumor formation in vivo using a murine model. Male athymic nude mice (6 weeks old) were procured from the Experimental Animal Center at Guangxi Medical University in Nanning, China. All animals were housed under standard conditions in the center's animal care facility. Ethical approval for all animal experimental protocols was obtained from the Guangxi Medical University Animal Care and Use Committee, ensuring compliance with relevant ethical guidelines for animal research. To establish the tumor model, SMMC7721 tumor cells stably transfected with either a negative control (NC) or circR-4600 were resuspended in 200 μl of phosphate-buffered saline (PBS) and injected via the tail vein into each mouse (with five mice per group; an additional mouse was used to assess model efficacy). Prior to injection, circR-4600 overexpression was confirmed using reverse transcription quantitative polymerase chain reaction (RT-qPCR). After 3-4 weeks post-injection, humane euthanasia was performed on all mice. Lung metastasis was evaluated through photographic assessment, while hematoxylin and eosin (H&E) staining was employed to assess the engraftment of HCC cells in the lung tissue. Furthermore, we quantified the expression levels of E-cadherin (E-cad), matrix metalloproteinase 9 (MMP9), and Ki-67 in lung tissues using RT-qPCR. Immunohistochemistry and immunoblotting were utilized for validation. Each experiment was repeated three times to ensure the reliability of our results.

Proteomic Analysis of circR-4600 Pulldown

The biotin-labeled RNA was synthesized *in vitro* using the MEGAscriptTM T7 Kit (Invitrogen, USA), with the incorporation of Bio-16-UTP (10 mM, Ambion) during transcription. Subsequently, 2 μl of DNase I was added, and the reaction mixture was incubated at 37℃ for 15 minutes to remove DNA. Following this, 2 μl of 0.2 M EDTA was added. To facilitate the formation of secondary RNA structures, the biotin-labeled RNA (1 μg) was heated at 95℃ for 2 minutes, followed by incubation on ice for 3 minutes and further incubation at room temperature in RNA structure buffer for 30 minutes. Magnetic beads (Invitrogen, USA) were utilized for RNA binding and enrichment. The folded RNA was then mixed with extracts from HCC cells in 500 μl of RIP wash buffer. The magnetic beads were resuspended in 50 μl of RIP wash buffer, followed by the addition of Dynabeads M-280 streptavidin (60210, Invitrogen), and incubated at 4℃. After centrifugation for 1 minute, the supernatant was discarded. The beads were washed with RIP wash buffer and boiled in SDS buffer. Pulled-down proteins were detected using western blotting and mass spectrometry. The RNA probes used were as follows: circR-4600 sense: taatacgactcactatagggCTGGCCTCGTCATCCGCCCACCTTGGAGATAGGCTCTCGCTCTGTCACC;antisense:taatacgactcactatagggGGAATAGGCTCTCGCTCTGTCACCTGGCCTCGTCATCCGCCCACCTTG.

Western blotting (WB) analysis

WB analysis was performed to detect protein expression levels. Proteins were extracted from both cellular and tissue samples using cell lysis buffer (9803, CST) following the manufacturer's protocol. Protein concentrations were determined using the BCA protein concentration assay kit (Beyotime, China). Subsequently, proteins were separated by SDS-PAGE gel electrophoresis and transferred onto PVDF membranes. After blocking the membranes with 5% non-fat milk, they were incubated overnight at 4℃ with specific primary antibodies (such as GAPDH, Vimentin, E-cadherin, MMP9, DVL3, P62, DAB2, etc., diluted at 1 : 1000). Following primary antibody incubation, membranes were then incubated with appropriate secondary antibodies for 1 hour. Finally, images were captured using the Odyssey CLX dual-color infrared imaging system.

RIP-qPCR detects the interaction between DVL3 and circR-4600

The RIP (RNA-Binding Protein Immunoprecipitation) experiment was conducted using the RIP RNA-Binding Protein Immunoprecipitation kit (Sigma, USA) according to the manufacturer's instructions. Initially, cells were collected from the cell culture plate and transferred to centrifuge tubes. Subsequently, 100 μl of RIP lysis buffer was added to the cell pellet. The lysate was then incubated on ice for 5 minutes followed by overnight incubation at 4℃. Upon thawing, the lysate was centrifuged at 14,000 rpm for 10 minutes at 4℃. Next, 100 μl of the supernatant was mixed with 900 μl of RIP immunoprecipitation buffer (comprising 860 μl of RIP wash buffer, 35 μl of 0.5 M EDTA, and 5 μl of RNase inhibitor). DVL3 antibody (Abcam) was bound to magnetic beads and then incubated overnight at 4℃ with the cell lysate under gentle rotation. Following five washes, purified precipitated RNA and proteins were obtained for analysis. WB was employed to confirm the specificity of the DVL3 antibody. RT-qPCR was utilized to detect RNA enriched by DVL3 to elucidate its interaction with circR-4600.

Analysis of the relationship between DVL3 expression and prognosis in HCC using The Cancer Genome Atlas (TCGA) database

In this study, mRNA expression data and clinical information of HCC patients were retrieved from TCGA, and differentially expressed genes associated with OS were identified, with a specific focus on the DVL3 gene. Differential expression of DVL3 in HCC patients was visualized using box plots. Based on the expression levels of DVL3, HCC patients were stratified into high-expression and low-expression groups, and Kaplan-Meier survival curves were employed for visualization to assess the relationship between DVL3 and the prognosis as well as OS rate of HCC.

Immunofluorescence analysis

The expression levels of LC3B and P62 were examined using immunofluorescence. Cell slides were placed in 6-well plates and cells were seeded onto them, then cultured at 37℃ with 5% CO2 until reaching appropriate density. After cell attachment, fixation was performed using 4% paraformaldehyde at room temperature for 10 minutes, followed by permeabilization with PBS containing 0.25% Triton X-100 for 10 minutes. Subsequently, nonspecific binding sites were blocked with PBS solution containing 1% BSA for 30 minutes. Then, primary antibodies against LC3B (3868, CST) and P62 (23214, CST) were incubated overnight at 4℃ at a dilution ratio of 1 : 1000. The next day, cells were washed three times with PBS for 5

minutes each, followed by incubation with corresponding fluorescently labeled secondary antibodies (diluted at 1:500) for 1 hour. A 50 µl drop of anti-fade mounting medium (containing DAPI) (S2110-5-solarbiol) was placed on a coverslip, and cells from the slides were positioned in the mounting medium to avoid air bubbles. Finally, fluorescent microscopy was employed to observe and capture images for the analysis of LC3B and P62 expression levels.

Statistical analysis

Quantitative data were categorized based on their distribution into normal and non-normal distributions. Data with a normal distribution were presented as mean ± standard deviation (SD), while non-normally distributed data were presented as median and interquartile range. For normally distributed data, comparisons between two groups were conducted using Student's t-test. For non-normally distributed data, comparisons were performed using the Wilcoxon rank-sum test. For comparisons among multiple groups, one-way analysis of variance (ANOVA) followed by Tukey's honest significant difference test. Total survival rates were computed using the Kaplan-Meier method, with differences in survival assessed using the log-rank test. All statistical analyses and visualizations were performed using GraphPad Prism 9, SPSS 23.0, and R Studio software. In statistical analysis, a significance level of $P < 0.05$ indicated statistical significance, $P < 0.01$ denoted highly significant differences, and $P < 0.001$ signified extremely significant differences.

Results

HCC patients with low circR-4600 expression present poor prognosis

To further screen for significantly differentially expressed circRNAs in HCC, circRNA microarray analyses were conducted on six pairs of HCC and adjacent non-tumor tissues to delineate the aberrantly regulated circRNA expression profile in HCC (Figure 1A). To validate the microarray analysis results, several promising circRNAs were selected for RT-qPCR validation, and the results were generally consistent with those of the microarray analysis. Particularly, hsa_circRNA_104600 (also known as hsa_circ_0005927, circR-4600) exhibited significantly downregulated expression in HCC tissues compared to adjacent non-tumor tissues (Figure 1B).

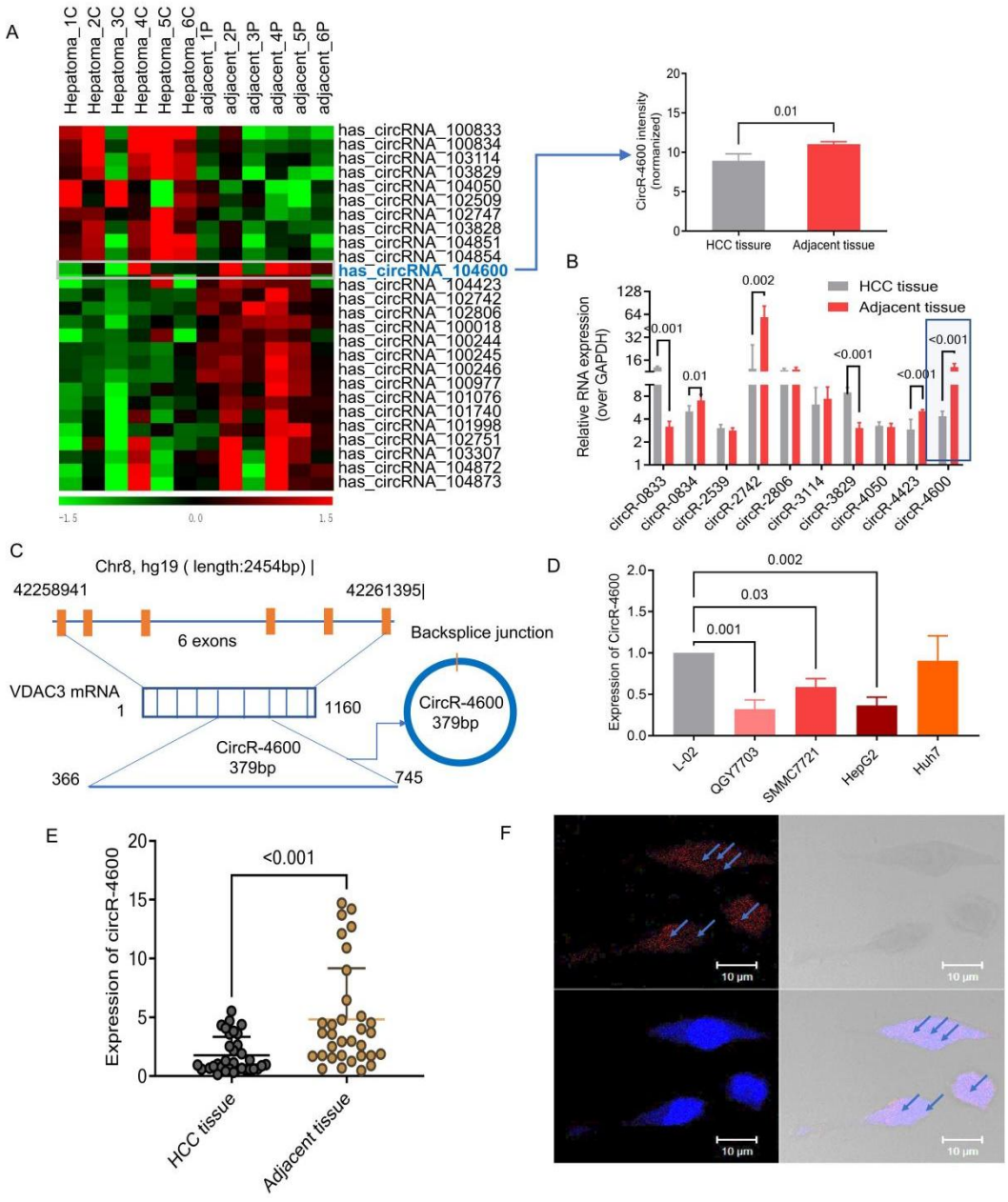

Figure 1. Low expression of CircR-4600 in HCC. (A) Analysis of CircRNA microarray. Aberrantly regulated circRNAs are depicted in a heatmap, with green indicating low expression and red indicating high expression. The expression level of circR-4600 is downregulated in HCC tissues. (B) A few potential circRNAs are validated by RT-qPCR. (C) The parental gene of circR-4600, mRNA, and the circular structure model are presented. (D) The expression level of circR-4600 in different HCC cell lines is examined by RT-qPCR (n = 3). (E) The expression level of circR-4600 in 33 cases of HCC tissues and adjacent cancer tissues is validated by RT-qPCR. (F) The localization of circR-4600 in HCC cells is detected by FISH experiments, with circR-4600 primarily located in the cytoplasm.

The parental gene of circR-4600 is VDAC3, a protein located in the outer mitochondrial membrane, crucial for ion channel function, especially in cellular metabolism and energy generation processes. Additionally, VDAC3 plays a critical role in maintaining mitochondrial function under oxidative stress conditions[19]. The VDAC3 gene is located on human chromosome 8, and its transcript is a 1160 bp mRNA. Within this mRNA, a 379 bp sequence forms the circular structure of circR-4600 through back-splicing junction (BSJ) (Figure 1C). To delve deeper into the expression of circR-4600 in different HCC cell lines, RT-qPCR analysis was performed on L02, QGY7703, SMMC7721, HepG2, and Huh7 cell lines. The results showed a significant downregulation of circR-4600 expression in QGY7703, SMMC7721, and HepG2 cell lines compared to L02 cells ($P < 0.05$), as depicted in Figure 1D. Subsequently, 33 pairs of HCC and corresponding adjacent non-tumor tissue samples were collected, revealing that circR-4600 expression levels were generally lower in HCC tissues than in adjacent non-tumor tissues, consistent with the observed expression pattern in cell lines (Figure 1E). Furthermore, FISH detection confirmed that circR-4600 primarily localized to the cytoplasm (Figure 1F).

Following the initial identification and molecular characterization of circR-4600, we further examined its clinical significance regarding dysregulation. We analyzed circR-4600 expression in a well-characterized HCC patient cohort to assess its correlation with tumor progression and clinical outcomes. 222 pairs of HCC samples and corresponding adjacent non-tumor tissues were collected. RT-qPCR was utilized for quantitative analysis of circR-4600 expression levels. Based on the median relative expression level of circR-4600 in tumor tissues, samples were divided into high-expression and low-expression groups (Figure 2A). The study results revealed a significant decrease in circR-4600 expression in HCC tissues compared to adjacent non-tumor tissues ($P < 0.001$, Figure 2B). Prognostic evaluation of HCC patients using the Kaplan-Meier method indicated that low circR-4600 expression portended poorer prognosis compared to the high-expression group, manifested by significantly lower OS rates ($P < 0.05$, Figure 2C). The baseline characteristics of the 222 HCC patients are presented in Tables 1 and 2. These findings suggest that low expression of circR-4600 in HCC tissues may be closely associated with adverse patient prognosis.

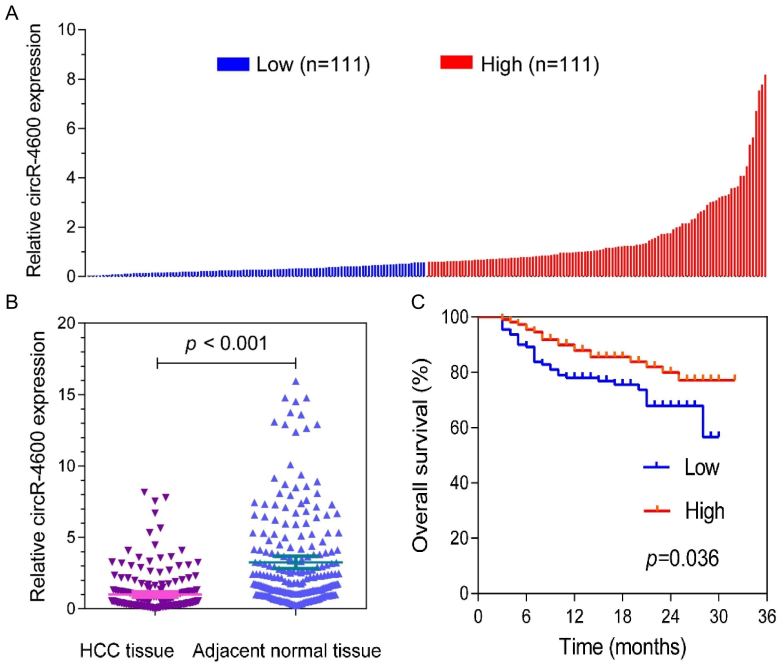

Figure 2. Low expression of circ-4600 in HCC indicates poor prognosis. (A) A total of 222 HCC samples were collected. The expression level of circR-4600 was quantitatively analyzed using RT-qPCR. Based on the median relative expression level of circR-4600 in tumor tissues, the samples were divided into high-expression and low-expression groups. (B) The expression level of circR-4600 in HCC tissues and adjacent cancer tissues was validated by RT-qPCR. (C) Survival analysis was conducted using the Kaplan-Meier method for prognostic evaluation of HCC patients. Patients were divided into high-expression and low-expression groups based on the median relative expression level of circR-4600 in HCC tissues. The x-axis represents survival time, while the y-axis represents the overall survival rate.

Table 1. Relationships between circR-4600 expression and clinical data of HBV-related HCC patients.

Variables	CircR-4600 expression				Survival analysis		
	Low (n=111)	High (n=111)	OR(95%CI)	*P*	Patients	HR*(95%CI)	*P**
Sex				0.702			0.485
Female	17	15	1.16 (0.55-2.45)		32	Ref.	
Male	94	96	Ref.		190	1.36 (0.58-3.18)	
Age (years)				0.170			0.155
< 60	86	94	0.62 (0.32-1.23)		180	Ref.	
≥ 60	25	17	Ref.		42	0.54 (0.23-1.26)	
Size (cm)				0.882			**0.002**
< 5cm	31	32	0.96 (0.53-1.72)		63	Ref.	
≥ 5cm	80	79	Ref.		159	4.89 (1.76-13.58)	
Number				0.252			0.340
< 3	98	103	0.59 (0.23-1.47)		201	Ref.	
≥ 3	13	8	Ref.		21	1.12 (0.65-3.56)	
Tumor capsule				0.587			0.309
Complete	62	66	0.86 (0.51-1.47)		128	Ref.	
Incomplete/absent	49	45	Ref.		94	1.34 (0.76-2.36)	
Lymph node metastasis				0.325			**0.002**
No	100	104	0.61 (0.23-1.64)		204	Ref.	
Yes	11	7	Ref.		18	3.19 (1.55-6.58)	
Vascular invasion				0.478			**0.000**
No	71	76	0.57 (0.47-1.43)		147	Ref.	
Yes	40	35	Ref.		75	2.78 (1.59-4.85)	
Microvascular invasion				0.077			**0.001**
No	40	53	0.62 (0.36-1.01)		93	Ref.	
Yes	71	58	Ref.		129	3.39 (1.69-6.78)	
AFP				0.893			**0.034**
< 400	53	54	0.97 (0.57-1.63)		107	Ref.	
≥ 400	58	57	Ref.		115	1.87 (1.05-3.34)	
BCLC stage				0.686			**0.009**
0+A	50	53	0.90 (0.53-1.52)		103	Ref.	
B+C	61	58	Ref.		119	2.24 (1.22-4.10)	
CircR-4600 expression				NA			**0.036**
Low	111	0			111	Ref.	
High	0	111			111	0.54 (0.31-0.96)	

Table 2. Survival of the HBV-related HCC patients with differentially expressed circR-4600.

Variables	Patients	MST(months)	Crude HR (95% CI)	*P*	Adjusted HR* (95%CI)	*P**
Size (cm)				**0.002**		**0.043**
< 5cm	63	18	Ref.		Ref.	
≥ 5cm	159	17	4.89 (1.76-13.58)		3.04 (1.04-8.92)	
Lymph node metastasis				**0.002**		0.065
No	204	17	Ref.		Ref.	
Yes	18	13	3.19 (1.55-6.58)		2.04 (0.96-4.35)	
Vascular invasion				**< 0.001**		0.140
No	147	18	Ref.		Ref.	
Yes	75	15	2.78 (1.59-4.85)		1.61 (0.86-3.02)	
Microvascular invasion				**0.001**		0.074
No	93	19	Ref.		Ref.	
Yes	12	16	3.39 (1.69-6.78)		1.99 (0.94-4.23)	
AFP				**0.034**		0.345
< 400	107	18	Ref.		Ref.	
≥ 400	115	16	1.87 (1.05-3.34)		1.34 (0.73-2.45)	
CircR-4600 expression				**0.036**		**0.041**
Low	111	16	Ref.		Ref.	
High	111	18	0.54 (0.31-0.96)		0.55 (0.31-0.97)	

circR-4600 inhibits HCC cell proliferation, migration, and invasion

To investigate the role of circR-4600 in HCC cell proliferation, migration, and invasion, a circR-4600 overexpression system was constructed using the pCDH-CMV-MCS-EF1-GFP+Puro (CD513B-1) vector. Control (non-transfected cells), negative control (NC, i.e.,

pCDH group), and circR-4600 overexpression plasmids were transfected into 293T cells, and total RNA was extracted for RT-qPCR analysis of circR-4600 expression levels. The results demonstrated significantly higher expression levels in the circR-4600 overexpression group compared to the control and NC groups, thereby validating the successful construction of the overexpression system (Figure 3A). The specific primers for circR-4600 (divergent primers) were as follows: Forward: 5'-tagaacttctctctaaaga-3', Reverse: 5'-cgaaattattctgtgacagtt-3'. To confirm that the amplified product was circR-4600, sequencing analysis was performed to detect reads matching the BSJ site. The results showed that the amplified product matched the circR-4600 sequence and contained the BSJ site, further confirming the accuracy of the overexpression system (Figure 3B). Subsequently, the overexpression system of circR-4600 was applied to HepG2 and SMMC7721 cells. BrdU assay showed that the proliferation ability of cells overexpressing circR-4600 was significantly lower than that of the control and NC groups, especially in SMMC7721 cells (Figure 3C-D). CCK-8 assay yielded similar results (Figure 3E). Plate clone formation assay further confirmed a significant reduction in the number of clones in SMMC7721 cells after overexpression of circR-4600 (Figure 3F). These data indicate that overexpression of circR-4600 inhibits HCC cell proliferation. To further investigate the impact of circR-4600 on the migration and invasion ability of HCC cells, transwell invasion assay and scratch wound healing assay were conducted. The results showed that the invasion ability of cells overexpressing circR-4600 was significantly reduced, with a decrease in the number of cells crossing the matrigel and membrane (Figure 3G). The scratch assay also demonstrated that the migration speed of cells overexpressing circR-4600 was significantly slower than that of the control and NC groups (Figure 3H). Therefore, by constructing and applying the circR-4600 overexpression system in HCC cells, we found that overexpression of circR-4600 significantly inhibits HCC cell proliferation, migration, and invasion. These results indicate that circR-4600 plays a suppressive role in HCC cell proliferation, migration, and invasion.

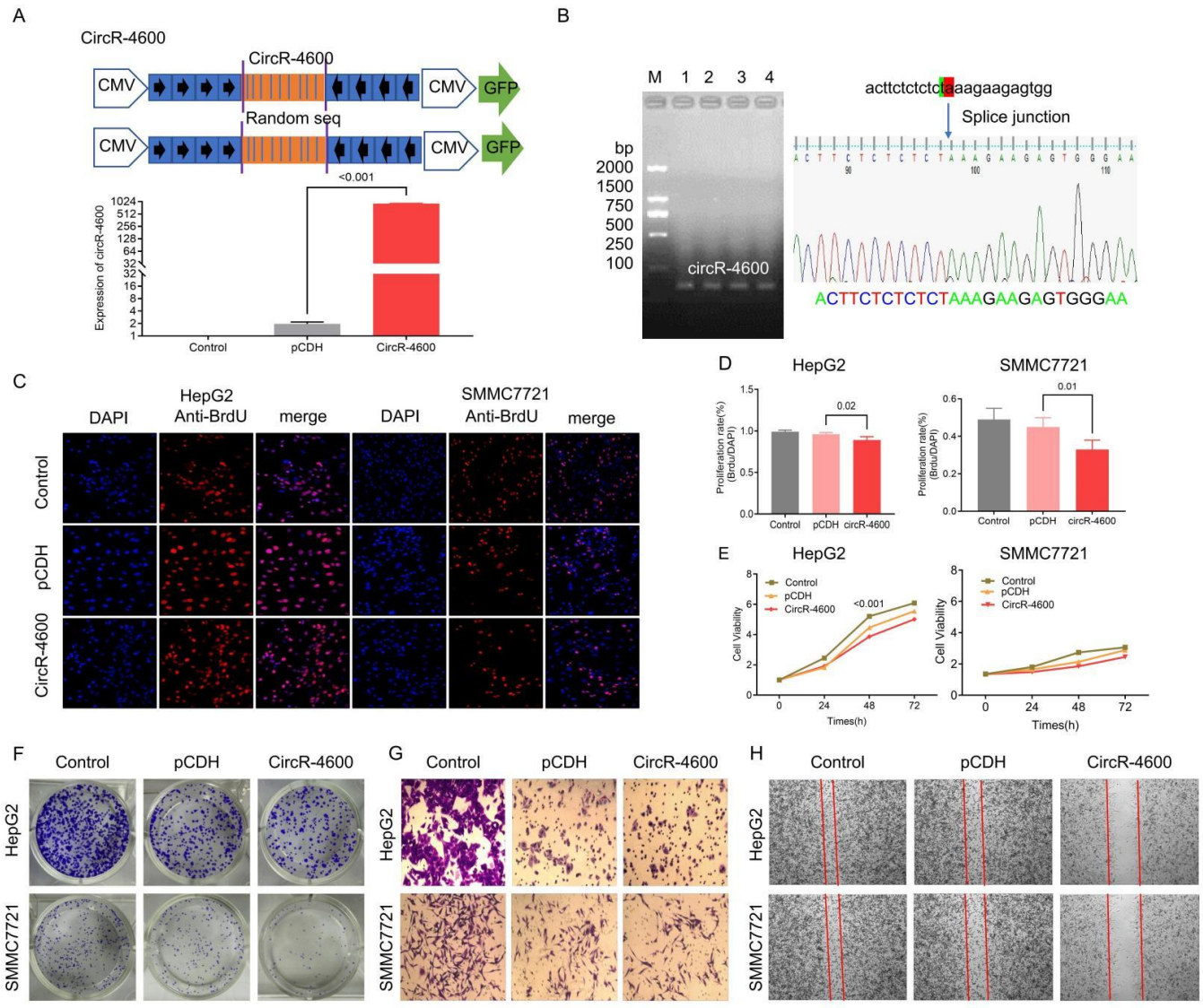

Figure 3. CircR-4600 suppresses proliferation, migration, and invasion of HCC cells. (A) An overexpression system for circR-4600 was constructed using the pCDH-CMV-MCS-EF1-GFP+Puro (CD513B-1) vector. Control indicates non-transfected cells, while the pCDH group represents cells transfected with empty vector as a negative control. (B) The overexpression system was validated. Sequence analysis confirmed that the amplified product was consistent with the circR-4600 sequence and that a BSJ site was present. (C-D) The BrdU assay was used to detect the level of cell proliferation. Cells overexpressing circR-4600 demonstrated significantly lower proliferation ability than the control group and NC group, especially in SMMC7721 cells (n = 3). (E) The CCK-8 assay was used to detect cell proliferation ability (n = 3). (F) The plate clone experiment was conducted to determine the clone formation rate. A significant reduction in the number of cell clones was observed in SMMC7721 cells after overexpression of circR-4600 (n = 3). (G) The Transwell method was used to determine cell invasion. Cells overexpressing circR-4600 showed a significant

reduction in invasion ability, with fewer cells passing through the Matrigel gel and filter membrane (n = 3). (H) The scratch test was used to detect cell migration ability. Cells overexpressing circR-4600 migrated at a significantly slower speed than the control group and NC group (n = 3).

circR-4600 inhibits *in vivo* lung metastasis

To investigate the role of circR-4600 in HCC cell metastasis, a mouse lung metastasis model was established by tail vein injection of SMMC7721 cells stably overexpressing circR-4600 into 6-week-old athymic male nude mice (Figure 4A). Mice in the NC group were examined at the 3rd and 4th weeks to observe liver and lung metastasis. Compared to the NC group, mice in the circR-4600 overexpression group exhibited significantly reduced lung metastatic lesions, indicating an inhibitory effect of circR-4600 on intrahepatic cholangiocarcinoma cell metastasis *in vivo* (Figure 4B). Subsequently, H&E staining was performed to assess tumor cell lung metastasis. Tumor tissues in the NC group showed pronounced heterogeneity, disordered arrangement of cancer cells, and loss of normal structure and polarity, suggesting a higher incidence of tumor cell invasion compared to the circR-4600 group (Figure 4C). RT-qPCR results revealed higher levels of E-cad and lower levels of Ki67 and MMP9 in the circR-4600 overexpression group (Figure 4D). IHC staining and WB were performed to specifically label Ki67, MMP9, and E-cad proteins. In lung metastatic lesions of mice overexpressing circR-4600, the number of Ki67-positive cells (indicating actively proliferating tumor cells) was significantly reduced, while the expression of MMP9 (a proteinase closely associated with tumor invasion and metastasis) was suppressed. Concurrently, the expression of E-cad (a protein involved in maintaining intercellular adhesion) was markedly enhanced (Figure 4E-F). These findings collectively suggest that circR-4600 inhibits the proliferation, invasion, and metastasis of HCC cells *in vivo*.

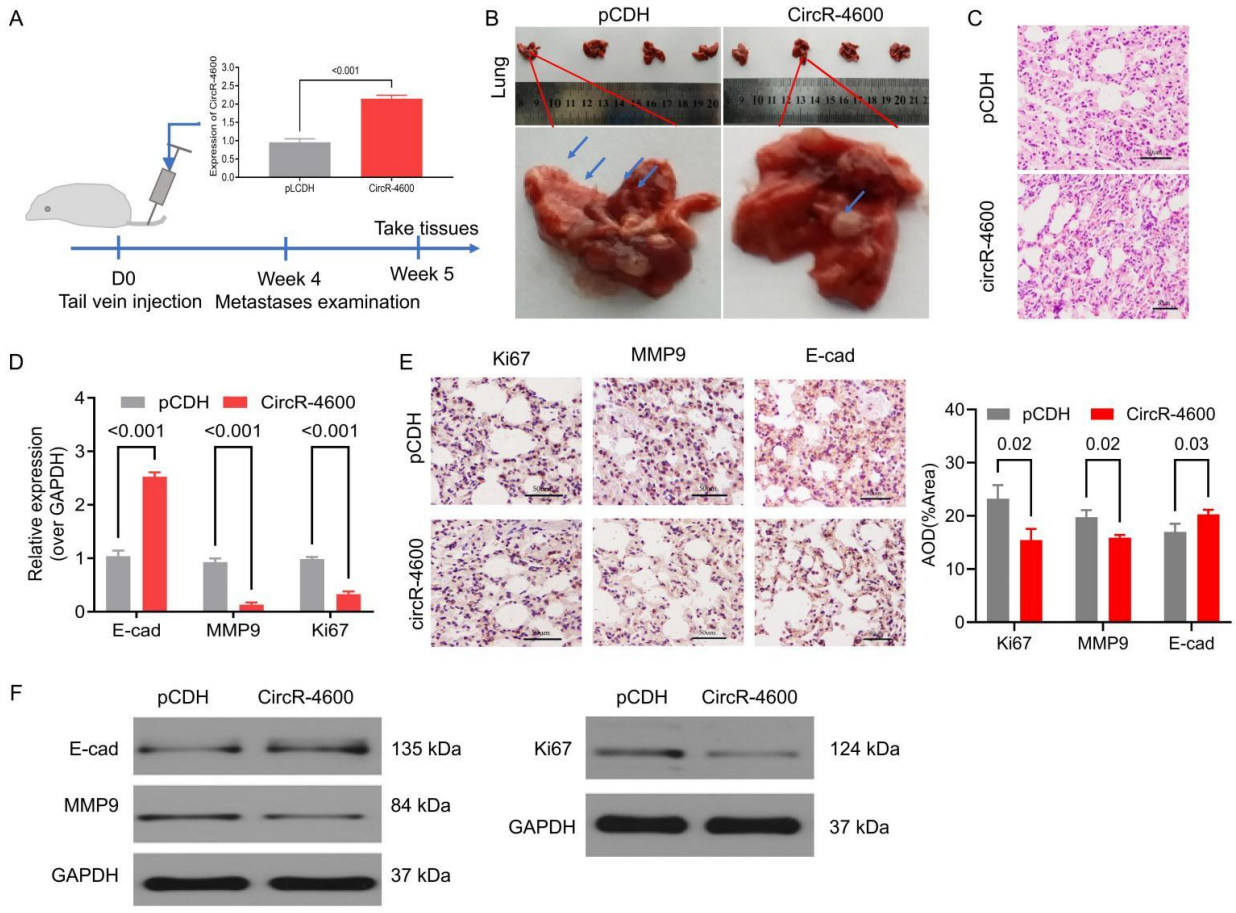

Figure 4. CircR-4600 suppresses *in vivo* lung metastasis. (A) A timeline of the mouse lung metastasis model was established by injecting SMMC7721 cells stably overexpressing circR-4600 into the tail vein of 6-week-old athymic male nude mice. (B) The level of lung metastasis of HCC cells in different groups was examined. Compared to the NC group, the number of lung metastatic lesions in mice from the circR-4600 overexpression group was significantly reduced. (C) H&E staining was used to assess the lung metastasis of HCC cells. The tumor tissue structure in the NC group showed significant heterogeneity, with disordered arrangement of cancer cells, loss of normal structure and polarity, indicating that the invasion of tumor cells was higher than in the circR-4600 group. (D) RT-qPCR showed that E-cad levels were higher in the circR-4600 overexpression group, while Ki67 and MMP9 levels were lower (n = 5). (E-F) The expression levels of E-cad, Ki67, and MMP9 in lung tissue were detected by IHC, and WB. IHC staining and WB method were used to specifically label Ki67, MMP9 and E-cad proteins. In lung metastatic lesions of mice overexpressing circR-4600, the number of ki67-positive cells was significantly reduced, while the expression of MMP9 was inhibited. Meanwhile, the expression of E-cad was significantly enhanced (n = 5).

circR-4600 regulates HCC progression through interaction with DVL3

Based on the results from FISH analysis, we observed the expression of circR-4600 in the cytoplasm. This finding suggests that circR-4600 may interact with cytoplasmic proteins, potentially influencing their biological functions. To further investigate the interaction between circR-4600 and cytoplasmic proteins, we conducted a circR-4600 RNA pulldown experiment. In this experiment,

we used sense and antisense probes for circR-4600 and identified relevant proteins using ESI-FT-ICR-MS technology (Figure 5A). Among the identified interacting proteins, DVL3 exhibited significant binding activity with circR-4600. Notably, DVL3 plays a crucial role in regulating malignant behaviors of tumors, including cell proliferation, migration, epithelial-mesenchymal transition (EMT), and stemness[20,21]. This discovery provides a novel perspective on the functional role of circR-4600 in cells. Furthermore, RIP-qPCR experiments using DVL3 antibody confirmed the interaction between DVL3 and circR-4600. RT-qPCR analysis of precipitated RNA validated the presence of circR-4600 (Figure 5B). Additionally, RT-qPCR analysis revealed the impact of circR-4600 overexpression on DVL3 mRNA levels, showing a significant decrease with increasing circR-4600 expression. This was further confirmed by WB experiments, demonstrating that circR-4600 overexpression led to a decrease in DVL3 protein levels (Figure 5C). Collectively, these results indicate a negative regulatory relationship between circR-4600 and DVL3. Furthermore, we constructed DVL3 inhibition plasmids and found that both circR-4600 overexpression and DVL3 inhibition decreased DVL3 expression levels. When cells were simultaneously overexpressed with circR-4600 and inhibited DVL3, DVL3 levels were reduced to the lowest extent (Figure 5D). Overall, these data emphasize the significant interaction between DVL3 protein and circR-4600, providing important clues for understanding their cellular function.

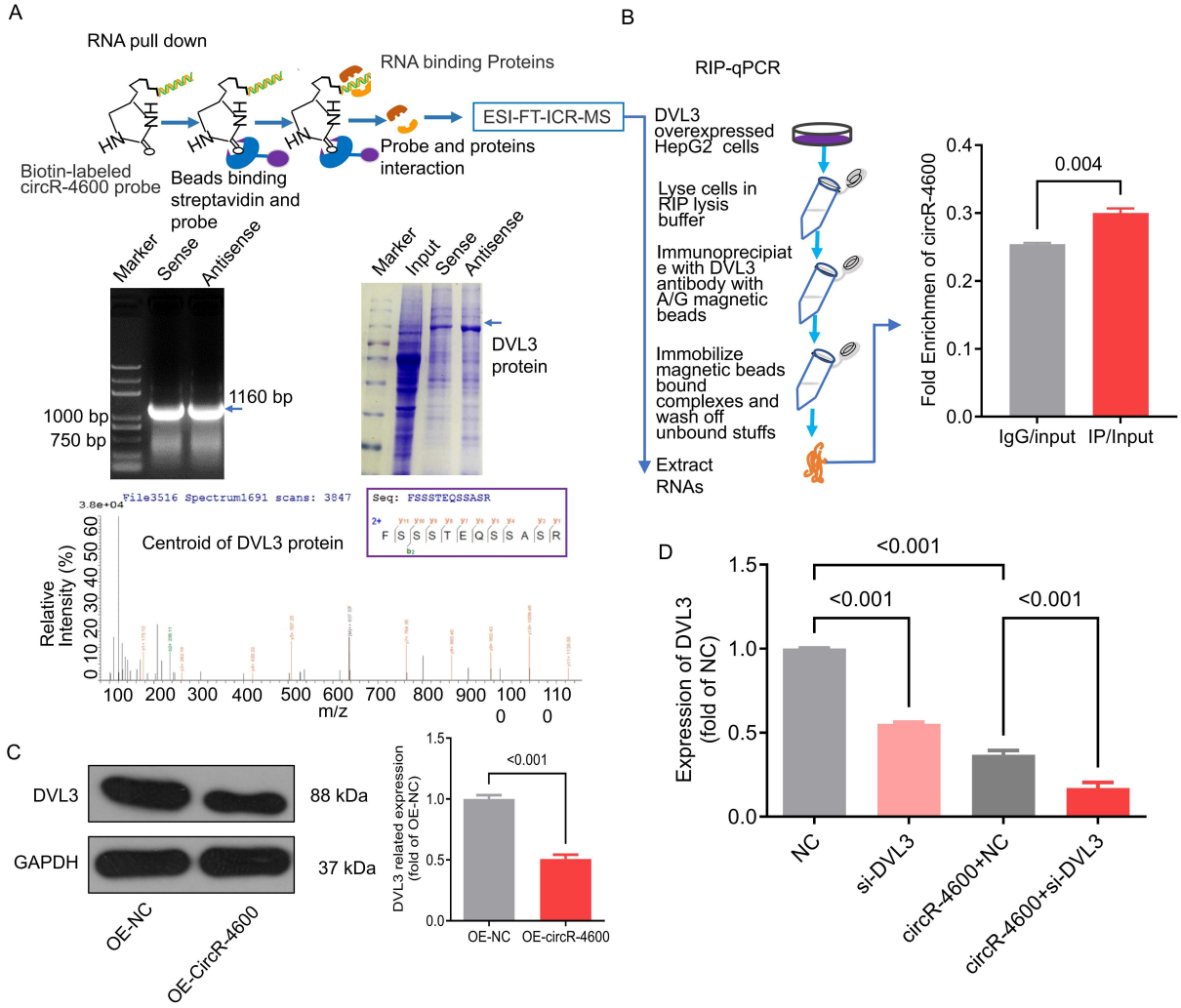

Figure 5. CircR-4600 regulates HCC progression through interaction with DVL3. (A) Potential interacting proteins were identified using the circR-4600-RNA pull-down experiment and ESI-FT-ICR-MS technology. (B) The interaction between DVL3 and circR-4600 was measured by RIP-qPCR. After immunoprecipitation with a DVL3 antibody, RT-qPCR analysis of the precipitated RNA was performed to verify the expression of circR-4600. (C) The effect of circR-4600 overexpression on DVL3 levels was detected by RT-qPCR and WB experiments. With the increase in circR-4600 expression, a significant decrease in DVL3 levels was observed (n = 3). (D) Both overexpression of circR-4600 and inhibition of DVL3 could reduce the expression level of DVL3. When cells overexpressed circR-4600 and inhibited DVL3 at the same time, the level of DVL3 dropped to the lowest (n = 3).

Upregulation of DVL3 correlates with enhanced proliferation, invasion abilities, and altered autophagy levels in HCC cells

We collected 35 samples of HCC tissues along with their corresponding adjacent tissues. The results demonstrated a significant upregulation of DVL3 expression in HCC tissues compared to adjacent tissues, consistent with the analysis from TCGA database (Figure 6A). Survival analysis further revealed a significant decrease in OS in HCC patients with high DVL3 expression levels compared to those with low expression ($P < 0.05$, Figure 6A). *In vitro* experiments showed that DVL3 inhibition markedly attenuated the proliferation capability of HCC cells (Figure 6B). Transwell invasion assays further confirmed that DVL3 inhibition weakened the

invasive ability of HCC cells, as evidenced by a significant decrease in the number of cells passing through matrigel-coated membranes (Figure 6C). Additionally, DVL3 inhibition reduced the expression of Vimentin and increased E-cad expression, suggesting that DVL3 inhibition may suppress the invasive and migratory abilities of HCC cells and EMT process (Figure 6D). Previous studies have indicated that autophagy-related genes WDFY3 and ALFY can clear DVL3 aggregates through the autophagy pathway, thereby playing a role in disease progression[22,23]. Based on these findings, we examined the effects of DVL3 inhibition on HCC cell autophagy using immunofluorescence and WB techniques. DVL3 inhibition significantly reduced LC3B expression and increased P62 levels, suggesting inhibited autophagic activity (Figure 6E). Further investigation revealed that overexpression of circR-4600 or inhibition of DVL3 could both suppress the expression of LC3B and promote P62 accumulation. When cells were simultaneously overexpressed with circR-4600 and inhibited DVL3, autophagic activity decreased to even lower levels (Figure 6F), providing new insights into the role of DVL3 in HCC development.

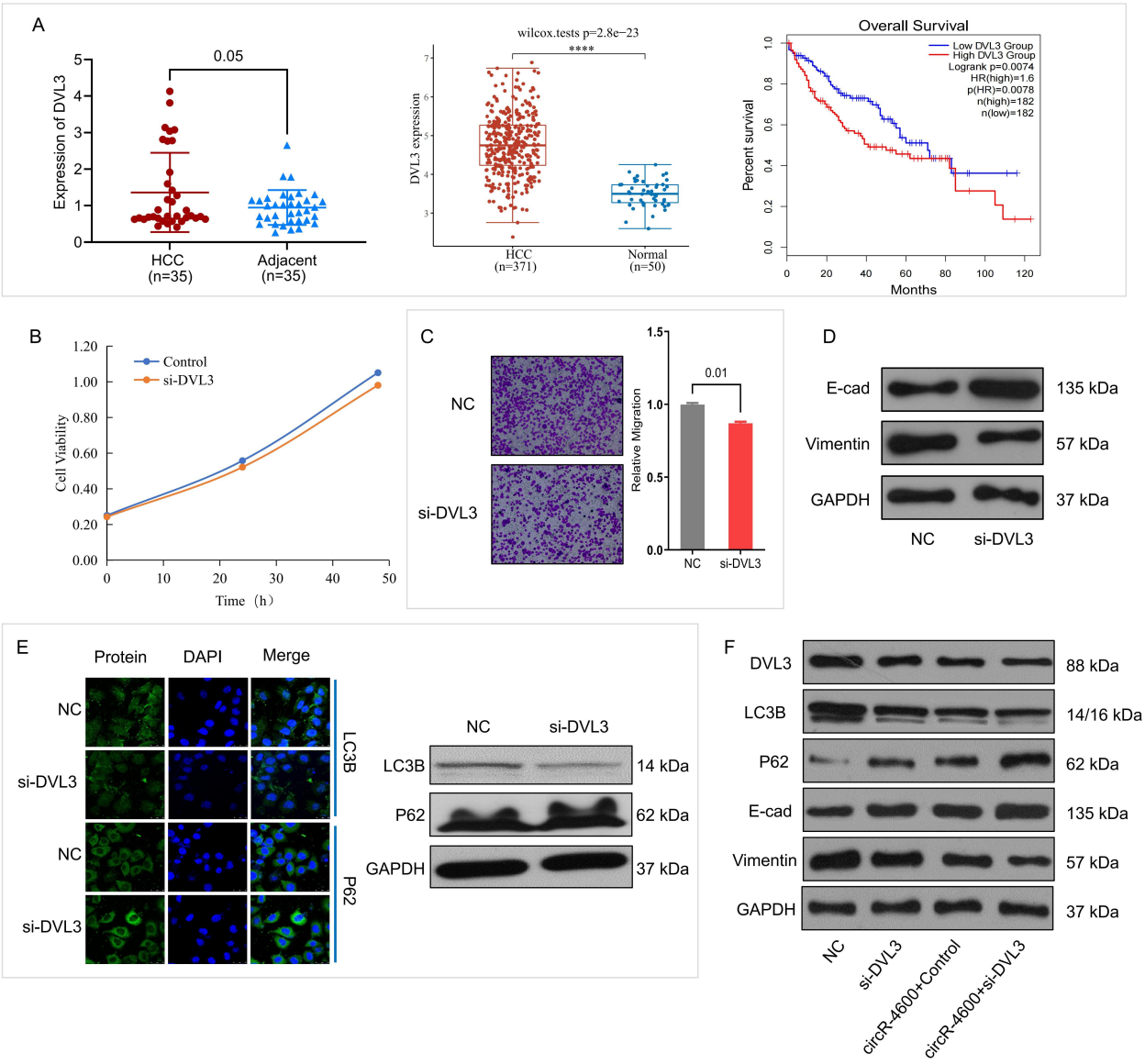

Figure 6. Upregulation of DVL3 is associated with enhanced proliferation and invasion capabilities of HCC cells, and affects the level of cellular autophagy. (A) RT-qPCR was used to detect the expression level of DVL3 in 35 cases of HCC tissues and their corresponding para-cancerous tissues. At the same time, mRNA expression data and clinical information of HCC patients were collected from the TCGA database. The expression level of DVL3 in HCC tissues was significantly higher than that in normal tissues. The Kaplan-Meier method was used for prognosis assessment of HCC patients. According to the median relative expression level of DVL3 in HCC tissues, patients were divided into high expression group and low expression group. The horizontal axis represents survival time, and the vertical axis represents overall survival rate. (B) The CCK-8 experiment was used to detect the level of cell proliferation. The inhibition of DVL3 significantly weakened the proliferation ability of HCC cells. (C) The Transwell method was used to determine cell invasion. The inhibition of DVL3 weakened the invasion ability of HCC cells, and the number of cells passing through Matrigel gel and filter membrane was significantly reduced (n = 3). (D) WB was used to detect the expression level of E-cad and Vimentin in HCC cells (n = 3). (E-F) Immunofluorescence and WB experiments were used to detect the effect of DVL3 inhibition on autophagy of HCC cells. The inhibition of DVL3 significantly reduced the expression of LC3B and increased the level of P62. Overexpression of circR-4600 or inhibition of DVL3 could inhibit the expression of LC3B and promote the accumulation of P62. When cells overexpressed circR-4600 and inhibited DVL3 at the same time, the autophagy activity dropped to a lower level (n = 3).

ATG5 plays a crucial role in cellular autophagy, participating not only in the formation of autophagosomes and fusion with lysosomes but also regulating the autophagic process, providing an efficient mechanism for cellular recycling and stress response. As a core member of the autophagy-related protein family, ATG5, together with other proteins, forms the basic framework of autophagy. In this study, by constructing ATG5 inhibition plasmids, we found that ATG5 inhibition significantly reduced the migration and invasion

capabilities of HCC cells (Figure 7A). Moreover, ATG5 inhibition decreased autophagy levels, manifested by reduced LC3B and increased P62 levels, while also inhibiting the invasive abilities of HCC cells and the EMT process, indicated by downregulation of E-cad and upregulation of Vimentin (Figure 7B). When ATG5 and DVL3 were simultaneously inhibited, autophagic activity was further reduced, accompanied by increased E-cad and decreased Vimentin, suggesting reduced invasive and migratory abilities of HCC cells and restoration of epithelial-like characteristics (Figure 7C).

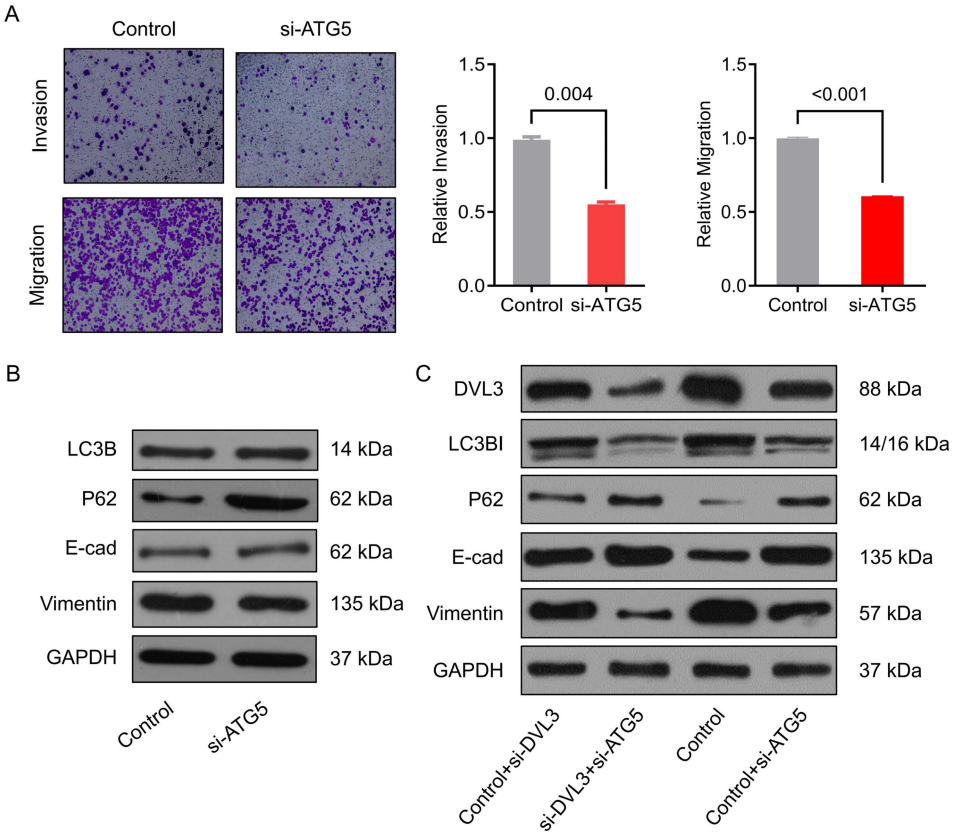

Figure 7. ATG5 treatment regulates the invasion and autophagy level of HCC cells. (A) The Transwell method was used to determine cell invasion. The inhibition of ATG5 significantly reduced the invasion ability of HCC cells (n = 3). (B-C) The inhibition of ATG5 reduced the level of autophagy, manifested as a decrease in LC3B and an upregulation of P62, and also inhibited the invasion ability and EMT process of HCC cells, specifically manifested as a downregulation of E-cad and an upregulation of Vimentin. When ATG5 and DVL3 were inhibited at the same time, the autophagy activity was further reduced, accompanied by an increase in E-cad and a decrease in Vimentin (n = 3).

DAB2 protein participates in HCC Cell invasion, metastasis, and autophagy regulation

Previous studies have revealed that downregulation of DAB2 protein expression is closely associated with the occurrence and progression of various human malignancies. Additionally, DAB2 can interact with Beclin-1, promoting Beclin-1 phosphorylation to regulate autophagosome assembly, thereby influencing the autophagic process[24,25]. Interestingly, in our previous circR-4600 RNA pulldown experiments, DAB2 protein exhibited binding activity with circR-4600. Based on this, we performed RIP-qPCR experiments using DVL3 antibody in HCC cells overexpressing DVL3 to elucidate the interaction between DVL3 and DAB2. RT-qPCR analysis of precipitated RNA confirmed the presence of DAB2 (Figure 8A). Furthermore, in DVL3-inhibited HCC cells, DAB2 expression was significantly increased (Figure 8B). In the 35 HCC tissue samples collected, DAB2 expression levels were significantly elevated in adjacent tissues, consistent with the analysis from TCGA database (Figure 8C). Survival analysis further indicated a significant decrease in OS in patients with high DAB2 expression levels compared to those with low DAB2 expression ($P < 0.05$, Figure 8C). Overall, in HCC cells, circR-4600 overexpression leads to the inhibition of DVL3 expression through its interaction with both DVL3 and DAB2. Consequently, this inhibition suppresses ATG5-mediated cellular autophagy, as evidenced by reduced LC3B levels and increased P62 levels. As a result, HCC cell invasion and metastatic capabilities decline, and epithelial-like features are restored. Additionally, DAB2 may participate in autophagy regulation by interacting with Beclin-1, further influencing HCC cell invasion, metastasis, and the EMT process (Figure 8D).

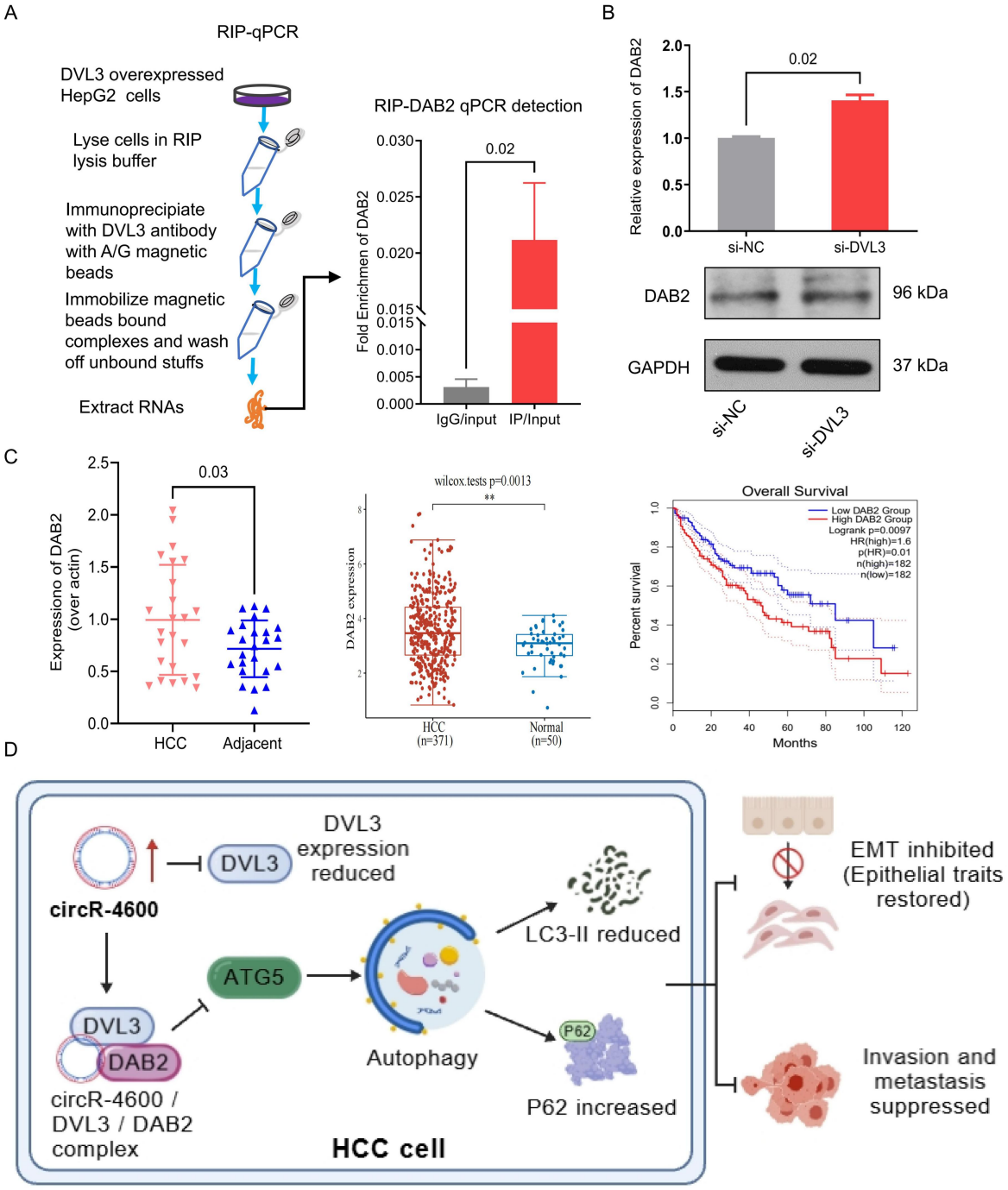

Figure 8. DAB2 protein is involved in the regulation of HCC cell invasion, metastasis, and cellular autophagy. (A-B) The interaction between DVL3 and DAB2 was determined by RIP-qPCR. After immunoprecipitation with DVL3 antibody, the precipitated proteins were tested by WB to verify the expression of DAB2 (n = 3). (C) RT-qPCR was used to detect the expression level of DAB2 in HCC tissues and their corresponding para-cancerous tissues. At the same time, mRNA expression data and clinical information of HCC patients were collected from the TCGA database. The expression level of DAB2 in HCC tissues was significantly higher than that in normal tissues. The Kaplan-Meier method was used for prognosis assessment of HCC patients. According to the median relative expression level of DAB2 in HCC tissues, patients were divided into high expression group and low expression group. The horizontal axis represents survival time, and the vertical axis represents overall survival rate. (D) Schematic diagram of circR-4600 suppressing hepatocellular carcinoma metastasis by interaction with DVL3 via ATG5-mediated autophagy. In HCC cells, when circR-4600 is overexpressed, circR-4600 interacts with DVL3 and DAB2, inhibits the expression of DVL3, and subsequently inhibits ATG5-mediated cellular autophagy, manifested as a decrease in LC3B and an increase in P62, thereby inhibiting the invasion and metastasis ability and EMT process of HCC cells, leading to a decrease in the invasion and metastasis ability of HCC cells and the recovery of epithelial characteristics. At the same time, DAB2 may also participate in the regulation of autophagy through interaction with Beclin-1, thereby affecting the invasion, metastasis, and EMT process of HCC cells. Created with BioGDP.com.

Discussion

In this study, we identified a circular RNA called circR-4600 with significant implications in HCC. The expression level of circR-4600 in HCC tissues was consistently lower compared to adjacent tissues, consistent with the observed expression pattern in HCC cell lines. Prognostic evaluation of HCC patients using the Kaplan-Meier method revealed that the low expression of circR-4600 in HCC tissues may be closely associated with adverse patient outcomes. In *in vivo* experiments, we found that

circR-4600 significantly inhibited the *in vivo* metastasis of HCC cells, indicating its role in suppressing the proliferation, invasion, and metastasis of HCC cells *in vivo*. Further research revealed that circR-4600 could interact with the DVL3 protein, thereby inhibiting DVL3 expression. DVL3 protein plays a crucial role in regulating the malignant behavior of tumors, including cell proliferation, migration, EMT, and stemness. Consistent with the mechanistic findings, TCGA-based analyses revealed that DVL3 is significantly upregulated in human HCC, exhibiting an expression pattern opposite to that of circR-4600. Although a direct correlation analysis could not be performed using paired clinical specimens, this population-level evidence further supports the biological relevance of the circR-4600-DVL3 regulatory axis in hepatocellular carcinoma. Additionally, we discovered the interaction between the DAB2 protein and circR-4600. The downregulation of DAB2 expression is closely associated with the occurrence and progression of various human malignancies. DAB2 can interact with Beclin-1 to regulate autophagosome assembly by promoting Beclin-1 phosphorylation, thereby affecting the autophagy process. In HCC cells, overexpression of circR-4600 inhibited DVL3 expression through its interaction with both DVL3 and DAB2, subsequently suppressing ATG5-mediated cellular autophagy, as evidenced by decreased LC3B and increased P62 levels. This ultimately led to the inhibition of HCC cell invasion and metastasis capabilities and restoration of epithelial-like characteristics. Overall, these findings elucidate the significant role of circR-4600 in HCC and its mechanism of regulating HCC progression through interaction with DVL3 and DAB2. These findings highlight circR-4600 as a previously unrecognized regulator of autophagy in HCC and suggest its potential translational relevance.

Previous studies have indicated that DVL3 serves as an element of the WNT signaling pathway, mediating resistance to IGFIR inhibition by modulating IGF-RAS signaling. Specific enhancement of sensitivity to IGFIR inhibition can be achieved through genetic or pharmacological blockade of DVL3. In breast and prostate cancer cells, this sensitivity is associated with heightened MEK-ERK activation and relies on both MEK activity and DVL3 expression. DVL3 exists within an adapter complex linking IGFIR to RAS, wherein the complex also encompasses DAB2; dual blockade of DVL and DAB2 can synergistically activate ERKs and render cells sensitive to IGFIR inhibition[26]. In another study, the N-terminal domain of DAB2 interacts with the signaling mediator DVL3 of the WNT pathway. WNT stimulation leads to time-dependent dissociation of endogenous DAB2-DVL3 interaction in fibroblast cells, while overexpression of DAB2 results in loss of maintenance of DAB2-DVL3 association[27]. This underscores potential significant roles of DVL3 and DAB2 in cancer initiation and progression. Given that DVL3 is a central component of the canonical Wnt/β-catenin signaling pathway, it is reasonable to speculate that circR-4600-mediated downregulation of DVL3 may influence Wnt/β-catenin activity, thereby contributing to the suppression of EMT observed in this study. Although EMT-related phenotypic changes and marker alterations were clearly demonstrated, direct assessment of active (non-phosphorylated) β-catenin and its downstream targets, such as c-Myc and Cyclin D1, was not performed. Future studies incorporating these analyses will be important to further delineate the involvement of Wnt/β-catenin signaling in the circR-4600-DVL3 regulatory axis and to refine the mechanistic link between DVL3 downregulation and EMT inhibition. Furthermore, based on the general regulatory mechanisms of circRNAs, potential underlying mechanisms may also involve protein stability and translation processes. Through binding to specific mRNAs, circRNAs enhance the stability and translation efficiency of these transcripts, thereby increasing the abundance of target proteins. The proteins translated from endogenous circRNAs participate in disease-related pathways, with some being translated into peptides through rolling circle translation. As miRNA sponges, circRNAs relieve the inhibitory effects of miRNAs on target mRNAs, thereby regulating protein translation. Alternatively, they may interact with RNA-binding proteins, influencing their interaction with target mRNAs. The nuclease resistance of circRNAs confers a long half-life, supporting their prolonged regulation of targets. This stability may contribute to the persistent regulation of DVL3, particularly under pathological conditions.

Regarding circR-4600, research has shown its upregulation in tumor tissues of lung cancer (LC) patients, significantly correlated with tumor size[28]. Microarray analysis of circRNA in plasma from colorectal cancer (CRC) patients reveals upregulation of circR-4600, correlating with clinical pathological features[29]. MetaDE analysis of circRNA expression profiles in gastric cancer (GC) identifies circR-4600 as a significantly downregulated differential circRNA, potentially serving as a more authentic biomarker for GC screening[30]. Overall, the altered expression of circR-4600 in LC, GC, and CRC suggests its association with tumorigenesis and progression. In this study, we observed a significant decrease in the expression of circR-4600 in HCC tissue relative to adjacent non-cancerous tissue, contrary to the upregulation observed in LC and CRC in existing studies. This finding suggests that circR-4600 may play different roles in different types of cancer. Therefore, further research is warranted to elucidate the specific functions and biological significance of circR-4600 in different tumors. Notably, a negative correlation between circR-4600 and DVL3 expression was observed in HCC tissues; however, the underlying molecular basis of this phenomenon remains to be fully elucidated. Functional interactions between circular RNAs and their binding proteins don't necessarily imply coordinated regulation at the transcriptional level. Accumulating evidence indicates that circRNAs predominantly regulate their interacting proteins through post-transcriptional or post-translational mechanisms, including modulation of protein stability, subcellular localization, or degradation pathways. In the present study, circR-4600 was shown to physically interact with DVL3 and suppress its protein expression, suggesting that circR-4600 may influence DVL3 abundance independently of transcriptional regulation. Given previous reports demonstrating that DVL3 can undergo selective degradation via autophagy-related pathways, it is plausible that circR-4600 participates in regulating DVL3 protein turnover or autophagy-mediated degradation, thereby contributing to their opposing expression patterns in HCC tissues. Thus, while the current data support a functional and regulatory association between circR-4600 and DVL3, the precise molecular mechanisms underlying their inverse expression trend warrant further investigation.

As a core protein of cellular autophagy, ATG5 exhibits altered expression in tumor cells, potentially influencing the level of autophagy and thereby affecting tumor growth and invasion. The role of cellular autophagy in promoting or inhibiting tumor invasion and metastasis depends on various factors, including tumor type, the level, and stage of autophagy, among others[31,32]. Furthermore, some studies have also found that ATG5 can impact tumor development by modulating cell death and survival signaling pathways[33,34]. In summary, DVL3, DAB2, ATG5, and cellular autophagy play pivotal roles in tumor invasion and metastasis. Elucidating the mechanisms by which DVL3, DAB2, and ATG5 regulate autophagy and developing targeted therap-

peutic strategies against these proteins could enhance tumor treatment outcomes. Moreover, these proteins may impact tumor invasiveness through other mechanisms as well.

However, this study does indeed have some limitations. Firstly, although the interaction between circR-4600 and DVL3 / DAB2 has been revealed, the detailed molecular mechanisms underlying this process still require further investigation. For instance, a deeper understanding of how circR-4600 specifically binds to DVL3 and DAB2, and how this binding affects their functions and activities, remains necessary. In this study, a classical rescue experiment - namely, DVL3 overexpression in the context of circR-4600 upregulation - was not performed, which limits the strength of causal inference regarding the circR-4600-DVL3 axis in hepatocellular carcinoma progression. Nevertheless, multiple independent and complementary lines of evidence were provided to support the biological relevance of this regulatory axis. Specifically, a significant negative correlation between circR-4600 and DVL3 expression was observed in clinical HCC specimens, and the two molecules exhibited opposing prognostic implications. Their physical interaction was confirmed by RNA pull-down and RIP assays. Moreover, consistent phenotypic effects were observed following circR-4600 overexpression or DVL3 inhibition in both *in vitro* and *in vivo* models. Notably, circR-4600 upregulation and DVL3 suppression converged on ATG5-mediated autophagy regulation and EMT-related pathways, further supporting the functional coherence of this axis. In addition, although autophagy-related changes were evaluated using established approaches such as LC3B and P62 expression analyses and immunofluorescence staining, these methods primarily reflect overall autophagy activity rather than dynamic autophagy flux. The mRFP-GFP-LC3B tandem fluorescent reporter has emerged as a powerful and widely accepted tool for real-time monitoring of autophagy flux, enabling discrimination between autophagosome formation and autolysosomal degradation. Application of this system would allow a more refined delineation of the specific autophagy stage regulated by the circR-4600-DVL3 axis, thereby further strengthening mechanistic resolution. Secondly, as a newly discovered circRNA in HCC invasion and metastasis, the application of circR-4600 in early HCC diagnosis and its value as a prognostic marker need longer-term validation. Lastly, despite the recognized significance of circR-4600 in HCC, its specific roles in other types of cancer remain unclear. Future investigations should comprehensively explore the expression and functional implications of circR-4600 across various cancer contexts to elucidate both its ubiquity and specificity in cancer biology.

Conclusion

The study investigated the role and mechanism of circR-4600 in HCC. Through circRNA microarray analysis, circR-4600 expression was downregulated in HCC tissues and correlated with poor prognosis. *In vitro* experiments demonstrated that overexpression of circR-4600 could inhibit HCC cell proliferation, migration, and invasion, consistent with *in vivo* study results. Furthermore, our research reveals that circR-4600 interacted with the DVL3 protein, inhibiting its expression and impacting HCC progression. Meanwhile, the DAB2 protein bound to circR-4600, participating in autophagy regulation, and influencing HCC cell invasion, metastasis, and the EMT process. Overall, this study revealed the significant role of circR-4600 in HCC and its potential molecular mechanisms, providing important clues for understanding its function within NPC cells.

Reference

1. Hou X, Liu W, Yang X, et al. Extracellular microparticles derived from hepatic progenitor cells deliver a death signal to hepatoma-initiating cells. J Nanobiotechnology, 2022, 20(1):79.
2. Yao J, Zhang X, Li J, et al. Silencing TRIP13 inhibits cell growth and metastasis of hepatocellular carcinoma by activating of TGF-beta1/smad3. Cancer Cell Int, 2018,18: 208.
3. El-Serag H B, Marrero J A, Rudolph L, et al. Diagnosis and treatment of hepatocellular carcinoma. Gastroenterology, 2008,134(6):1752-1763.
4. Debnath J, Gammoh N, Ryan K M. Autophagy and autophagy-related pathways in cancer. Nat Rev Mol Cell Biol, 2023,24(8):560-575.
5. Xiao Q, Liu H, Wang H S, et al. Histone deacetylase inhibitors promote epithelial-mesenchymal transition in Hepatocellular Carcinoma via AMPK-FOXO1-ULK1 signaling axis-mediated autophagy. Theranostics, 2020,10(22): 10245-10261.
6. Zhan Q, Liu B, Situ X, et al. New insights into the correlations between circulating tumor cells and target organ metastasis. Signal Transduct Target Ther, 2023,8(1):465.
7. Zhang K, Zhang L, Mi Y, et al. A ceRNA network and a potential regulatory axis in gastric cancer with different degrees of immune cell infiltration. Cancer Sci, 2020,111 (11):4041-4050.
8. Liu J, Liu H, Zeng Q, et al. Circular RNA circ-MAT2B facilitates glycolysis and growth of gastric cancer through regulating the miR-515-5p/HIF-1alpha axis. Cancer Cell Int, 2020,20:171.
9. Song X, Liang Y, Sang Y, et al. circHMCU Promotes Proliferation and Metastasis of Breast Cancer by Sponging the let-7 Family. Mol Ther Nucleic Acids, 2020,20:518-533.
10. Ji Y, Ni C, Shen Y, et al. ESRP1-mediated biogenesis of circPTPN12 inhibits hepatocellular carcinoma progression by PDLIM2/ NF-kappaB pathway. Mol Cancer, 2024,23(1): 143.
11. Hu X, Chen G, Huang Y, et al. Integrated Multiomics Reveals Silencing of has_circ_0006646 Promotes TRIM21-Mediated NCL Ubiquitination to Inhibit Hepatocellular Carcinoma Metastasis. Adv Sci (Weinh), 2024,11(16):e 2306915.
12. Wang X, Dong F L, Wang Y Q, et al. Exosomal circTGFBR2 promotes hepatocellular carcinoma progression via enhancing ATG5 mediated protective autophagy. Cell Death Dis, 2023,14(7):451.
13. Du A, Li S, Zhou Y, et al. M6A-mediated upregulation of circMDK promotes tumorigenesis and acts as a nanotherapeutic target in hepatocellular carcinoma. Mol Cancer, 2022,21(1):109.
14. Lin S, Zhuang J, Zhu L, et al. Matrine inhibits cell growth, migration, invasion and promotes autophagy in hepatocellular carcinoma by regulation of circ_0027345/miR-345-5p/HOXD3 axis. Cancer Cell Int, 2020,20:246.
15. Dai W, Liu Y, Zhang T, et al. Spindle function and Wnt

pathway inhibition by PBX1 to suppress tumor progression via downregulating DCDC2 in colorectal cancer. Oncogenesis, 2023,12(1):3.

16. Ali S R, Humphreys K J, Simpson K J, et al. Functional high-throughput screen identifies microRNAs that promote butyrate-induced death in colorectal cancer cells. Mol Ther Nucleic Acids, 2022,30:30-47.
17. Wang L, Chennupati R, Jin Y J, et al. YAP/TAZ Are Required to Suppress Osteogenic Differentiation of Vascular Smooth Muscle Cells. iScience, 2020,23(12):101860.
18. Li J, Liu X, Dong S, et al. Circ_0101802 Facilitates Colorectal Cancer Progression Depending on the Regulation of miR-665/DVL3 Signaling. Biochem Genet, 2022,60 (6):2250-2267.
19. Reina S, Nibali S C, Tomasello M F, et al. Voltage Dependent Anion Channel 3 (VDAC3) protects mitochondria from oxidative stress. Redox Biol, 2022,51:102264.
20. Li Z, Yang Z, Liu W, et al. Disheveled3 enhanced EMT and cancer stem-like cells properties via Wnt/beta-catenin/c-Myc/SOX2 pathway in colorectal cancer. J Transl Med, 2023,21(1):302.
21. Yang P, Zhang P, Zhang S. RNA-Binding Protein MEX3A Interacting with DVL3 Stabilizes Wnt/beta-Catenin Signaling in Endometrial Carcinoma. Int J Mol Sci, 2022,24(1).
22. Deneubourg C, Ramm M, Smith L J, et al. The spectrum of neurodevelopmental, neuromuscular and neurodegenerative disorders due to defective autophagy. Autophagy, 2022,18(3): 496-517.
23. Kadir R, Harel T, Markus B, et al. ALFY-Controlled DVL3 Autophagy Regulates Wnt Signaling, Determining Human Brain Size. PLoS Genet, 2016,12(3):e1005919.
24. Jiang Y, Woosley A N, Sivalingam N, et al. Cathepsin-B-mediated cleavage of Disabled-2 regulates TGF-beta-induced autophagy. Nat Cell Biol, 2016,18(8):851-863.
25. Tumbarello D A, Kendrick-Jones J, Buss F. Myosin VI and its cargo adaptors - linking endocytosis and autophagy. J Cell Sci, 2013,126(Pt 12):2561-2570.
26. Gao S, Bajrami I, Verrill C, et al. Dsh homolog DVL3 mediates resistance to IGFIR inhibition by regulating IGF-RAS signaling. Cancer Res, 2014,74(20):5866-5877.
27. Hocevar B A, Mou F, Rennolds J L, et al. Regulation of the Wnt signaling pathway by disabled-2 (Dab2). EMBO J, 2003,22(12):3084-3094.
28. Wang Y, Lu L J, Duan Y, et al. Analysis of circular RNA expression profiles of lung cancer in Xuanwei, China. J Clin Lab Anal, 2020,34(12):e23521.
29. Li J, Song Y, Wang J, et al. Plasma circular RNA panel acts as a novel diagnostic biomarker for colorectal cancer detection. Am J Transl Res, 2020,12(11):7395-7403.
30. Ding H X, Xu Q, Wang B G, et al. MetaDE-Based Analysis of circRNA Expression Profiles Involved in Gastric Cancer. Dig Dis Sci, 2020,65(10):2884-2895.
31. Chen Z, Lee H J, Kim H, et al. delta-Catenin promotes cell migration and invasion via Bcl-2-regulated suppression of autophagy in prostate cancer cells. Am J Cancer Res, 2022,12(1):108-122.
32. Korholz K, Ridinger J, Krunic D, et al. Broad-Spectrum HDAC Inhibitors Promote Autophagy through FOXO Transcription Factors in Neuroblastoma. Cells, 2021,10(5).
33. Mainz L, Sarhan M, Roth S, et al. Acute systemic knockdown of Atg7 is lethal and causes pancreatic destruction in shRNA transgenic mice. Autophagy, 2022,18 (12):2880-2893.
34. Celia A I, Colafrancesco S, Barbati C, et al. Autophagy in Rheumatic Diseases: Role in the Pathogenesis and Therapeutic Approaches. Cells, 2022,11(8).

Acknowledgements

We thank all participants involved in this study. Additionally, appreciation is extended to all researchers and clinical practitioners dedicated to HCC prevention and treatment efforts.

Author contributions

Conceptualization: Honglin Luo, Lequn Li, Gang Wang, Xiaosu Zou. Methodology: Honglin Luo, Gang Wang, Feixiang Wu. Validation: Gang Wang, Honglin Luo, Lequn Li. Formal analysis: Honglin Luo, Gang Wang, Shaoliang Zhu, Qiuxia Wei. Investigation: Gang Wang, Xiaofeng Dong, Shaoliang Zhu, Wenqian Nong, Qicong Chen, Hongwei Wang, Tao Yang, Ling Cai. Resources: Honglin Luo, Lequn Li. Data Curation: Honglin Luo, Gang Wang. Writing - original graft: Gang Wang, Honglin Luo. Writing - review & editing: Gang Wang, Honglin Luo, Feixiang Wu. Visualization: Gang Wang, Honglin Luo. Supervision: Honglin Luo, Feixiang Wu, Lequn Li. Project administration: Honglin Luo, Feixiang Wu, Lequn Li. Funding acquisition: Honglin Luo,Gang Wang.

Funding

The work was supported by Guangxi Natural Science Foundation Joint Special Project on Active Health and Common Diseases (2024GXNSFBA010103); National Natural Science Foundation of China (82360495); High-level Talent Scientific Research Startup Fund of People's Hospital of Guangxi Zhuang Autonomous Region (Guangxi Academy of Medical Sciences) (to Gang Wang: YKY-GCRC-202508); Research Initiation Grant for Elite Talent A at Guangxi Medical Science Academy, People's Hospital of Guangxi Zhuang Autonomous Region (YKY-GCRC-202303); Guangxi Young Elite Scientist Sponsorship Program (GXYESS2025053); Guangxi Zhuang Autonomous Region Disease Prevention and Control Science and Technology Project (GXJKKJ2025ZC048).

Animal Ethics declaration

Ethical approval for all animal experimental protocols was obtained from the Guangxi Medical University Animal Care and Use Committee, ensuring compliance with relevant ethical guidelines for animal research (approval number: LW2018038).

Human Ethics declaration

Ethical approval for population research was obtained from the Ethics Committee of Guangxi Academy of Medical Sciences (approval number: KY-GZR-2023-048).

Consent to Participate declaration

This study was approved by the Ethics Committee of Guangxi Academy of Medical Sciences. Owing to the retrospective nature of the study and the use of anonymized clinical specimens and data, the requirement for written informed consent was formally waived by the Ethics Committee of Guangxi Academy of Medical Sciences.

Availability of data and materials

Further inquiries of data and materials can be made directly to the corresponding author.

Patient consent for publication

Not applicable.

Competing interests

There are no conflicts of interest among the authors.

SUPPORTING MATERIALS

Additional supplementary information is available for download and review in the supplementary information section located on the right-hand side of this article's HTML page.

Supplementary Figure 1. Patient enrollment flowchart.

Supplementary Table 1. Sequences of primers**.**

Supplementary Table 2. Primers required for plasmid construction, lentivi ral packaging and verification.